Modeling and Model Updating of Torsional Behavior of an Industrial Steam Turbo Generator

Roberto Ricci[1]
e-mail: roberto1.ricci@mail.polimi.it

Paolo Pennacchi

Department of Mechanical Engineering,
Politecnico di Milano,
via La Masa 1,
20156 Milan, Italy

Emanuel Pesatori

Giorgio Turozzi

Department of R&D,
Franco Tosi Meccanica S.p.A.,
Piazza Monumento 12,
Legnano, 20025 Milan, Italy

The methods employed to perform rotordynamics calculations of industrial machines are rather standard and usually allow forecasting the dynamic behavior of the considered machines. Anyhow, in some cases, in order to obtain high level of accuracy, the model has to be updated to fit experimental results, and standard modeling methods have to be improved. In this paper, the updating of the torsional model of a steam turbogenerator is presented. In order to fit the eigenfrequencies calculated using the standard model and the natural frequencies measured on-field, a modeling improvement is proposed, considering partially the dynamics of the components usually modeled as rigid disks. The proposed method has also the aim to preserve the physical meaning of the model. Finally, the new model is updated, and a very good fitting is obtained between eigenfrequencies and experimental natural frequencies. [DOI: 10.1115/1.4000287]

Keywords: rotordynamic, model updating, torsional vibrations, natural frequencies

1 Introduction

During the operation of rotating machinery used in powerplants, some anomalies, such as electric faults, unusual conditions, or asymmetries in arc admission of steam in the turbine, can excite torsional vibrations. This condition is rather dangerous because normally torsional vibrations are not monitored. Moreover, if the torsional vibrations are characterized by frequencies closely related to blade row natural frequencies, blade modes could be excited with possible consequences on the blade integrity.

Therefore, during the design of the machine, besides the calculation of flexural eigenfrequencies and eigenmodes, also torsional ones are often calculated using a finite element model of the rotor train [1,2]. These eigenfrequencies are often different from the natural frequencies measured on-field; this means that in some cases the standard modeling method is not accurate enough. A modified method is proposed here, and the new model is subjected to a model updating procedure.

In the past decades, different authors studied the model updating procedure. Friswell and Mottershead [3] gave a fundamental contribution for structural dynamics. The model updating is generally based on the minimization of an objective function, which describes the difference between the model and the real system and it is characterized by three different aspects. The first one is the choice of the parameters that are optimized during the updating: These are the independent variables of the problem. Usually in rotordynamics uncertainty affects model parameters such as material properties, stiffness diameters of a generic element, or mass of a disk.

The second aspect that strongly characterizes the model updating is the algorithm used for the objective function minimization. Both mathematical and heuristic-probabilistic methods can be used to find the function minimum. Mathematical methods are proposed, for instance, in Refs. [4,5]. Genetic algorithms (GAs) and simulating annealing (SA) are the most used heuristic methods in literature Refs. [6–8].

The last aspect is the objective function. The choice of the function is strictly related to the parameters that can be experimentally extracted from the real system. The majority of the updating procedures proposed in literature considers both natural frequencies and mode shapes.

Unfortunately, for the experimental case considered in this paper—but almost generally for real rotating machinery—it was not possible to determine any experimental mode of the machine. Thus the model updating procedure requires the selection of the parameters to be updated on the basis of a sensitivity analysis and the setting of some constraints in order to preserve the physical meaning of the model. The obtained model is of the knowledge-based type, according to the classification given in Ref. [3] and the procedure described in Ref. [9].

2 In-Field Measurement of Torsional Natural Frequencies

The experimental tests were performed in a power plant. The unit considered was a 200 MW class steam turbogenerator with an approximate length of 24 m and a weight of 1,020,000 N operating at 3000 rpm (50 Hz) with one pole-pair generator. Steam expansion is realized in two different stages: high-intermediate pressure (HP-IP) and low pressure (LP) turbines.

Strain gauges were employed to measure torsional natural frequencies, but their location was constrained by machine layout. The only region easily accessible during normal machine operation was the one between the generator and the thrust bearing of HP-IP turbine, see Fig. 1. Two couples of strain gauges were placed on both sides of the rigid coupling to form one half-bridge and one full-bridge.

The signals of the strain gauges were transmitted by means of a telemetry collar, rigidly connected to the shaft, to a nearby fixed antenna. The frequency resolution was 0.73 Hz. Four torsional natural frequencies were determined; the values of which are reported in Table 1.

However, it is possible that not all the actual machine modes in the operating range were detected. In Sec. 3.3 it is shown that another eigenmode was present but was not detected. This can be explained by considering that the available measuring planes were two; they did not allow detecting the modes in which the measuring planes did not have relative motion. For the same reason, it was not possible to define also the experimental mode shapes.

It is worthy to note that these problems about modal analysis are commonly found in real rotating machinery and forces to perform modal updating using only data related to natural frequencies and not also to experimental mode shapes.

[1]Corresponding author.

Contributed by the Structures and Dynamics Committee of ASME for publication in the JOURNAL OF ENGINEERING FOR GAS TURBINES AND POWER. Manuscript received May 6, 2009; final manuscript received September 8, 2009; published online April 16, 2010. Assoc. Editor: James S. Wallace.

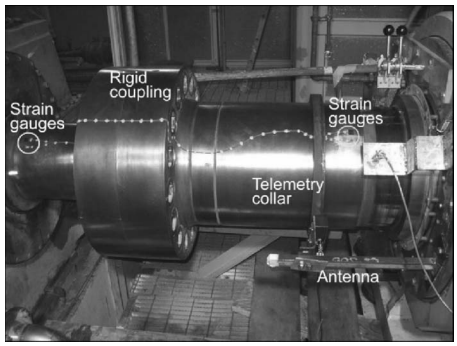

Fig. 1 Strain gauge installation

3 Rotor Modeling

Finite elements are used to model the machine presented in Sec. 2. First, the standard rotor dynamic method is introduced. The model of the shaft is set up using both consistent elements and lumped parameters. Then, the standard method is modified in order to take more accurately into consideration the effects of bladed disks and additional inertias on the eigenfrequencies.

3.1 Standard Torsional Finite Element Modeling. The *standard* finite element modeling (FEM) requires the discretization of the shaft and the result is shown in Fig. 2. Cylindrical parts are modeled by means of torsional beam elements with one degree of freedom (DOF) per node. In the modeling, the effects of step shafting on element stiffness have been accounted for.

The determination of both the inertia and the stiffness matrices is made using Lagrange's approach; the damping matrix is not defined because damping is normally negligible in torsional systems (further details can be found in Refs. [2,10,11]). A reference frame rotating at the rotating speed is adopted.

Table 1 Experimental natural frequencies

Experimental mode	Natural frequency (Hz)
Mode 1	10.8
Mode 2	27.7
Mode 3	123.5
Mode 4	144.0

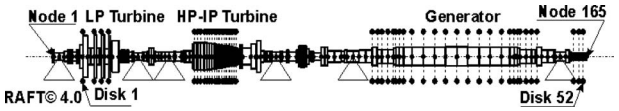

Fig. 2 Machine model

For a shaft element i of length l_i limited by the two end nodes i and $i+1$, the mass and stiffness matrices for the finite element approach can be expressed as [11]

$$[\mathbf{m}_i] = \frac{\rho_i I_{mi} l_i}{6}\begin{bmatrix} 2 & 1 \\ 1 & 2 \end{bmatrix} \tag{1}$$

$$[\mathbf{k}_i] = \frac{G_i I_{ki}}{l_i}\begin{bmatrix} 1 & -1 \\ -1 & 1 \end{bmatrix} \tag{2}$$

where ρ_i and I_{mi} indicate, respectively, the density and the polar moment of area calculated using the mass diameter of the ith element, whereas G_i and I_{ki} are the shear modulus and the polar moment of area of the ith element calculated using the stiffness diameter. The mass and stiffness matrices of the rotor shaft element are called *consistent*.

In order to take into account elements like bladed disks, fans, and the inertial effects of the copper bars in the generator/exciter (Fig. 2) *lumped* rigid disks are considered. This approach allows modeling a disk with a concentrated inertia J_{d_i} located in a general node i of the shaft-line (Fig. 3).

Because the disk is considered rigidly connected to a node belonging to the centroidal axis, it does not participate to torsional deformation and its stiffness matrix is not defined.

For a model composed of $n-1$ finite elements and n nodes, the vector of the generalized torsional displacement is

$$\boldsymbol{\theta}(t) = \{\theta_1(t), \ldots, \theta_n(t)\}^T \tag{3}$$

With this kind of modeling, the inertia matrix of the complete system $[\mathbf{M}]$ has a dimension of $n \times n$ and is a tri-diagonal matrix. On the main diagonal, the term J_{d_i} is present only if a disk is considered in the corresponding node.

$$[\mathbf{M}] = \begin{bmatrix} \frac{1}{3}\rho_1 I_{m1} l_1 + J_{d_1} & \frac{1}{6}\rho_1 I_{m1} l_1 & 0 & \cdots & 0 \\ \frac{1}{6}\rho_1 I_{m1} l_1 & \frac{1}{3}\rho_1 I_1 l_1 + \frac{1}{3}\rho_2 I_{m2} l_2 + J_{d_2} & \frac{1}{6}\rho_2 I_{m2} l_2 & \cdots & 0 \\ 0 & \frac{1}{6}\rho_2 I_{m2} l_2 & \frac{1}{3}\rho_2 I_{m2} l_2 + \frac{1}{3}\rho_3 I_{m3} l_3 + J_{d_3} & \cdots & 0 \\ \cdots & \cdots & \cdots & \ddots & \cdots \\ 0 & 0 & 0 & \cdots & \frac{1}{3}\rho_n I_{mn} l_n + J_{d_n} \end{bmatrix} \tag{4}$$

The fully assembled model stiffness matrix $[\mathbf{K}]$ is easier to define than the inertia one; in this case there are only the terms regarding the rotor elements. Similar to the inertia matrix $[\mathbf{M}]$, $[\mathbf{K}]$ is a tri-diagonal matrix:

$$[\mathbf{K}] = \begin{bmatrix} G_1 I_{k1}/l_1 & -G_1 I_{k1}/l_1 & 0 & \cdots & 0 \\ -G_1 I_{k1}/l_1 & G_1 I_{k1}/l_1 + G_2 I_{k2}/l_2 & -G_2 I_{k2}/l_2 & \cdots & 0 \\ 0 & -G_2 I_{k2}/l_2 & G_2 I_{k2}/l_2 + G_3 I_{k3}/l_3 & \cdots & 0 \\ \cdots & \cdots & \cdots & \ddots & \cdots \\ 0 & 0 & 0 & \cdots & G_n I_{kn}/l_n \end{bmatrix} \tag{5}$$

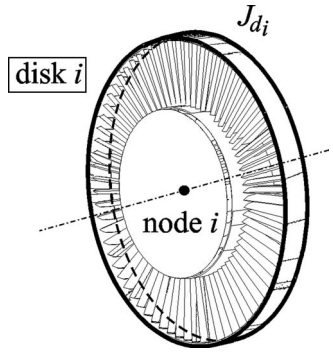

Fig. 3 Standard rigid disk

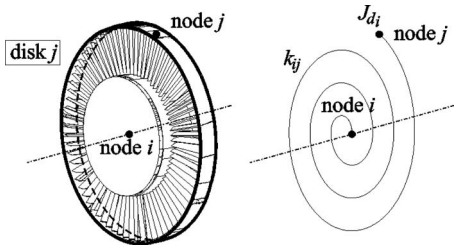

Fig. 4 Modified disk

This approach, easy to understand and to implement, has the disadvantage of a coarse representation of the dynamical behavior of the disks, especially if blade row modes are present. The consequence is that the complete model of rotor may result badly tuned. This notwithstanding the standard method is commonly used.

3.2 Modified Torsional Finite Element Modeling. The aim is to introduce into the model.

(1) The dynamic effects on torsional vibrations due to bladed row modes without considering a complete 3D FEM of the row and introducing a huge number of DOFs.
(2) The possible errors of the generator stiffness evaluation caused by the modeling of the copper bars by means of additional inertia only. This last modeling is generally performed without distinction for both flexural and torsional dynamic analyses. In the first case, this is generally correct because copper bars cause mainly inertial effects and their bending stiffness is negligible with respect to that of generator core (bars can also have relative motion in generator slots). In the second case, copper bars fill the slots and their torsional stiffness could be not negligible with respect to that of generator torsional elements. The consideration of lumped inertia for the copper bars completely neglects this aspect.

The proposed method considers an additional DOF for the disk, whose compliance should be considered, independent of the DOF of the node in which the disk is geometrically located. For simplicity, this corresponds to add an "additional" node in which the disk inertia is concentrated and which is not coincident with the nodes of the shaft elements.

In other words, while in the previous approach the disk was considered rigidly coupled with the shaft, in this case an additional node j, for a suitable graphical representation belonging to the plane orthogonal at the rotational axis and passing through the ith node, is included in the model (Fig. 4). The inertia of the disk is now considered concentrated in the new node, and the connection between the two nodes is modeled by means of a torsional spring.

This way, the number of DOFs of the model increases, but can be at maximum twice than before if a disk is considered per each node of the model. Moreover, the additional DOF can be used for some disks only; the dynamic effect of which is more relevant, while others can still be considered as rigid as before.

Indicating with m the number of the disks modeled by means of this approach, the vector of the generalized torsional displacement is

$$\boldsymbol{\theta}(t) = \left\{ \begin{array}{l} \underbrace{\theta_1(t), \ldots, \theta_i(t), \ldots, \theta_n(t), \ldots}_{\text{rotor nodes}} \\ \underbrace{\theta_{n+1}(t), \ldots, \theta_j(t), \ldots, \theta_{n+m}(t)}_{\text{additional (disks) nodes}} \end{array} \right\}^T \tag{6}$$

where n is the number of rotor nodes. Obviously, the DOF vector expansion also implies the increase in the dimension of fully assembled inertia and stiffness matrices of the system. To easily understand the changes in system matrices, we will use the new modeling for a disk only located in correspondence of the second node. The inertia matrix $[\mathbf{M}]$ has a shape similar to that of the standard modeling one (Eq. (4); in this case, however, its dimensions have increased, and the concentrated inertia related to the modified disk is put in the position associated with the additional DOF:

$$[\mathbf{M}] = \begin{bmatrix} \frac{1}{3}\rho_1 I_{m1} l_1 + J_{d_1} & \frac{1}{6}\rho_1 I_{m1} l_1 & 0 & \cdots & 0 & 0 \\ \frac{1}{6}\rho_1 I_{m1} l_1 & \frac{1}{3}\rho_1 I_1 l_1 + \frac{1}{3}\rho_2 I_{m2} l_2 & \frac{1}{6}\rho_2 I_{m2} l_2 & \cdots & 0 & 0 \\ 0 & \frac{1}{6}\rho_2 I_{m2} l_2 & \frac{1}{3}\rho_2 I_{m2} l_2 + \frac{1}{3}\rho_3 I_{m3} l_3 + J_{d_3} & \cdots & 0 & 0 \\ \cdots & \cdots & \cdots & \ddots & \cdots & \cdots \\ 0 & 0 & 0 & \cdots & \frac{1}{3}\rho_n I_{mn} l_n + J_{d_n} & 0 \\ 0 & 0 & 0 & \cdots & 0 & J_{d_2} \end{bmatrix} \tag{7}$$

where $[\mathbf{M}]$ is a $(n+m)\times(n+m)$ tri-diagonal matrix.

Converse to the standard method, the introduction of an additional DOF requires the definition of the connection of the disk to the shaft. This is made by the stiffness matrix of the jth disk that is proportional to the stiffness that characterizes the shaft element at which the disk is connected (Eq. (2)). Then the jth disk stiffness with respect to the stiffness of the ith element is

$$[\mathbf{k}_j] = \alpha_j \frac{G_i I_{ki}}{l_i} \begin{bmatrix} 1 & -1 \\ -1 & 1 \end{bmatrix} \tag{8}$$

On the basis of the DOF vector for the new modeling defined in Eq. (6), the fully assembled stiffness matrix of the system becomes

$$[\mathbf{K}] = \begin{bmatrix} G_1I_{k1}/l_1 & -G_1I_{k1}/l_1 & 0 & \cdots & 0 & 0 \\ -G_1I_{k1}/l_1 & G_1I_{k1}/l_1 + G_2I_{k2}/l_2 + \alpha_j G_2I_{k2}/l_2 & -G_2I_{k2}/l_2 & \cdots & 0 & -\alpha_j G_2I_{k2}/l_2 \\ 0 & -G_2I_{k2}/l_2 & G_2I_{k2}/l_2 + G_3I_{k3}/l_3 & \cdots & 0 & 0 \\ \cdots & \cdots & \cdots & \ddots & \cdots & \cdots \\ 0 & 0 & 0 & \cdots & G_nJ_{kn}/l_n & 0 \\ 0 & -\alpha_j G_2I_{k2}/l_2 & 0 & \cdots & 0 & \alpha_j G_2I_{k2}/l_2 \end{bmatrix} \tag{9}$$

and the stiffness matrix is no longer tri-diagonal. It is worthy to note that the proportionality stiffness coefficients α_i must be positive to have a consistent and physical meaning of disk stiffness matrix.

3.3 Eigenfrequency Calculation. After assembling the inertia and stiffness matrices of the machine, the eigenfrequencies can be calculated by means of the eigenvalue-eigenvector problem solution.

As stated by Cramer's rule, the system of dynamic equations of the free torsional vibrations of the rotor has nontrivial solutions if and only if the determinant of the coefficient matrix is equal to zero:

$$\det(\lambda^2[\mathbf{M}] + [\mathbf{K}]) = 0 \tag{10}$$

The left-hand side is the characteristic polynomial in the variable λ^2; its solutions, in terms of λ, are real numbers and represent the torsional eigenfrequencies of the considered system.

The original and standard torsional model of the machine presented in Sec. 2 is composed of 164 rotor elements and 52 lumped disks. It is worthy to note that disks are used for modeling both the machine blade stages and the additional mass due to the presence of copper bars in the generator. The sketch of the model is shown in Fig. 2, where the position of the disks is indicated by a dashed line with solid dots at the ends. The standard model has 165 DOFs and the calculated eigenfrequencies are shown in Table 2 and compared to the measured ones (i.e., Table 1).

Note that while modes 1 and 2 correspond to the first two experimental modes of Table 1, there is an eigenmode between experimental modes 2 and 3 (i.e., eigenmode 3 in Table 2), which was not detected on-field. Thus the fourth and fifth eigenmodes of Table 2 correspond, respectively, to the third and fourth modes detected during experimental measurements.

The third eigenmode non-identification can be easily explained by considering that the rotor part, in which the strain gauges are installed (dashed box in Fig. 5), rotates practically rigidly in eigenmode 3; thus the corresponding experimental mode cannot be detected using relative deformation measurements on this part.

This is a circumstantial evidence that the standard model is not completely wrong, even if the relative errors of the frequencies are not negligible, especially for the first mode. Considering the relative errors, it is worthy to note that the initial model underestimates the first three experimental natural frequencies (i.e., eigenfrequencies 1, 2, and 4 in Table 2) whereas overestimates the fourth natural frequency (i.e., eigenfrequency 5 in Table 2). This means that on one hand the determination of the eigenfrequencies is a non-linear problem and on the other hand the updating process should be able to modify the model parameters so that their effects on the first three eigenfrequencies would be opposite to the fourth one.

Table 2 Model eigenfrequencies

Eigenmode	Eigenfrequency (Hz)	Relative error (%)
Mode 1	8.89	−17.68
Mode 2	27.39	−1.11
Mode 3	82.12	N/A
Mode 4	118.36	−4.16
Mode 5	152.98	+6.23

4 Model Updating

As discussed in the Introduction, nearly all model updating methods consider the identified mode shapes or the experimental frequency response functions (FRFs). The knowledge and the use of these quantities guarantee that the updated model is correctly tuned and has a physical meaning.

In this case, it is impossible to measure experimental mode shapes or FRFs of the machine. Since the accessible parts during the operation are few, the only measured modal parameters are the natural frequencies.

The set of modal parameters $\mathbf{\Phi}$ that will be used for the model tuning process is then composed of four torsional natural frequencies already reported in Table 1 and can expressed in vector terms as

$$\mathbf{\Phi} = \{f_1, f_2, f_3, f_4\} \tag{11}$$

With regard to the independent variables of the problem, the hypothesis is that it is possible to define, on the basis of the standard modeling, which part of the real machine is badly modeled. As introduced in Sec. 3, the most probable errors could be the evaluation of the inertia of the bladed parts or of the stiffness of generator sections. The selection of the disks that will be considered in the modified model is performed after a sensitivity analysis.

Finally the constraints of the updating procedure are as follows.

- The differences between the updated eigenvalues and the natural frequencies are less than those of the initial model.
- Both the values of J_{d_i} and α_j are consistent: They must be positive.
- Both the values of J_{d_i} and α_j must be meaningful from a physical point of view: The variation range with respect to the nominal values will be limited.

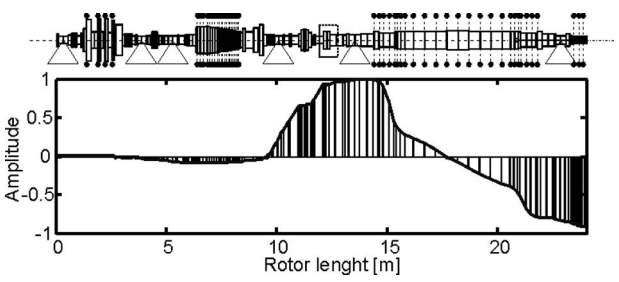

Fig. 5 Eigenmode 3—the dashed box indicates the strain gauge position on the rotor

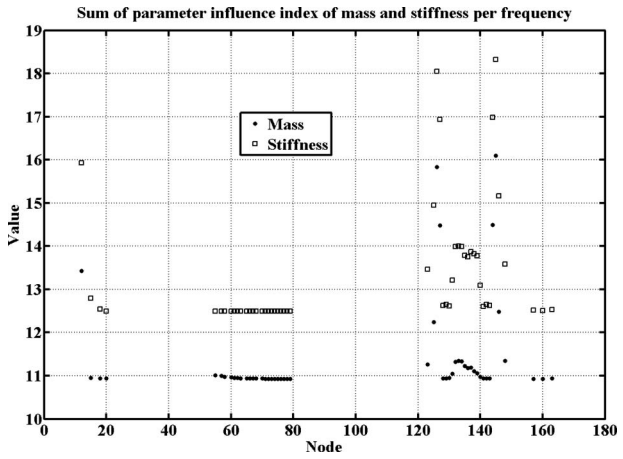

Fig. 6 Comprehensive effect of inertia and stiffness coefficients

4.1 Sensitivity Analysis. The determination of the most significant parameters of this model is performed by checking the effect on the eigenfrequencies, calculated with the standard model, caused by the variation in the disk inertia and stiffness, once the corresponding additional DOF is added.

Anyhow it is easy to understand that it is impossible to take into consideration the variation in an eigenfrequency only as a consequence of the variation in a single parameter. The determination of the eigenfrequencies is a non-linear problem, and each disk can cause variations in the opposite sign of model eigenfrequencies. A possible "rule of thumb" is the introduction of a merit index, which reveals the influence that each disk has on each eigenfrequency. This influence index is defined per each frequency as

$$i_{k,j} = \max_{\Delta}\left(\frac{f_{\Delta_j}^{(k)} - f_{0_j}}{f_{m_j} - f_{0_j}}\right), \quad 1 \le k \le n_d, \quad j \in \mathbf{\Phi} \tag{12}$$

where $f_{\Delta_j}^{(k)}$ is the jth eigenfrequency obtained for a percentage variation Δ of the independent variable k, f_{0_j} is the jth eigenfrequency of the standard model, and f_{m_j} is the corresponding experimental frequency.

The terms between parentheses in Eq. (12) represent the ratio between the eigenfrequency variation due to a parameter variation and the difference between the experimental and the standard model frequency values. For a more intuitive visualization the indices for each frequency have been summed up.

Since the aim of the study is the implementation of model updating processes that preserve the physical meaning of the starting model, the sensitivity analysis will be performed by establishing a variation of $\pm 20\%$ for the inertia parameters and 0–20% for the stiffness ones. Moreover the α_j coefficients are not considered to be equal to zero because in this case the eigenvalue problem is ill-conditioned due to the assembling of matrix $[\mathbf{K}]$ in Eq. (9).

The mass and stiffness global index trends are shown in Fig. 6. Considering the values assumed by these indices, the disk set taken into consideration for the model updating is composed of the disks located at the 12th (last stage of LP turbine), 125th, 126th, 127th, 144th, 145th, and 146th (generator) nodes.

With regard to the LP turbine, one could expect that the result of the optimization will set a low value for the corresponding α_j in order to decouple the blade row modes from the rotor. The results for the generator will be opposite in order to consider the torsional stiffness of the copper bars, and the updated values would respect the symmetry that the inertias have on the generator.

4.2 Optimization. As it was already said, since the modal parameters obtained by experimental tests are the torsional natural frequencies, the error function to be minimized will reflect the objective to fit the calculated eigenfrequencies to the measured natural frequencies. The fitting could be done in absolute or relative terms considering absolute or relative errors for each frequency:

$$\varepsilon_{a_j} = |f_{m_j} - \tilde{f}_j|, \quad \varepsilon_{r_j} = \frac{\varepsilon_{a_j}}{f_{m_j}} \tag{13}$$

where $\tilde{f}_j$ is the jth eigenfrequency of the model calculated with the updated parameters. Since the torsional frequencies identified by means of the experimental tests have different orders of magnitude, the objective function based on the relative error is more suitable than that on the absolute one. The relative error indeed assigns the same weight to the difference over each frequency and this allows tuning properly the model. Being the model updating process based on the minimization of the error associated with all the frequencies taken into consideration, the function to be minimized becomes

$$\varepsilon_r = \sum_{j \in \mathbf{\Phi}} \varepsilon_{r_j} \tag{14}$$

The independent variables of the problem are the moment of inertia and the stiffness coefficients of disks selected in Sec. 4.1; by defining

$$\Delta_{r0} = \sum_{j=1}^{4} \varepsilon_{rj} \tag{15}$$

the value assumed by the error function at the start of the updating process, the general optimization problem can be set as

$$\min \varepsilon_r(J_{d_j}, \alpha_j)$$

$$\text{subject to } \varepsilon_r < \Delta_{r0},$$

$$\tilde{J}_{d_j} > 0, \quad 1 \le j \le m$$

$$\frac{|J_{d_j} - \tilde{J}_{d_j}|}{J_{d_k}} \le 0.2, \quad 1 \le j \le m$$

$$0 < \alpha_j \le 0.2, \quad 1 \le j \le m \tag{16}$$

The problem in Eq. (16) is a mathematical constrained nonlinear optimization, in which the initial values are those contained in the matrix $[\mathbf{M}_d]$ for the moments of inertia and in the 0–20% range for the stiffness coefficients α_j. An iterative sequential quadratic programming (SQP) (quasi-Newton) method was adopted to solve the problem. For the sake of brevity, the complete description of the algorithm is not reported: Details can be found in Refs. [12,13]. The optimization process gives the optimal set of parameters fitting the measured torsional natural frequencies of the system.

According to the limits imposed during the sensitivity analysis, the allowed variations for updating parameters were $\pm 20\%$ for the moments of inertia and 0–20% for the stiffness coefficients. The algorithm stopped when the relative global error of Eq. (14) assumed the value of 2.28%. The eigenfrequencies obtained at the end of the updating are reported in Table 3. The optimal sets of parameter corresponding to the minimum found by the updating algorithm are shown in Figs. 7 and 8.

Note that the number of parameters employed is rather low. Disk moments of inertia variations are all negative. One of the most important variations is related to the 12th node, corresponding to the last stage of the LP turbine. This is consistent with the physical point of view since the uncertainty of inertia model can be easily related to this stage composed of long blades.

The physical correctness of the optimal stiffness parameters can be confirmed by noting the strong resemblance among the param-

Table 3 Eigenfrequencies after updating

Eigenmode	Natural frequency (Hz)	Eigenfrequency (Hz)	Relative error (%)
Mode 1	10.8	10.8	0
Mode 2	27.7	27.066	−2.28
Mode 3	123.5	123.5	0
Mode 4	144.0	144.0	0

eters associated with the generator additional inertia nodes. Stiffness ratios for these nodes tend to the maximum allowed by the optimization constraints and their values are about 19.5% of the corresponding stiffness coefficients of the rotor elements.

The first two updated eigenmodes, normalized with respect to the maximum amplitude, are shown in Figs. 9 and 10.

In the first eigenmode, as it can be noted in Fig. 9, the additional disk located in the last stage of the LP turbine appears completely uncoupled from the corresponding rotor element. This agrees with the value assumed by the stiffness coefficient after the updating process. The small stiffness coefficient involves the independence between the rotor and the disk DOFs.

The physical correctness of the previous statement has been verified by evaluating the stiffness of the disk by means of the product between its updated inertia and the square of the first eigenfrequency of the blade row calculated by means of 3D FEM.

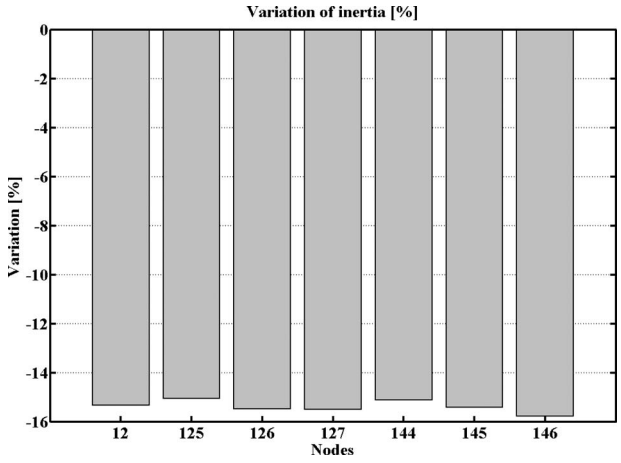

Fig. 7 Inertia variation

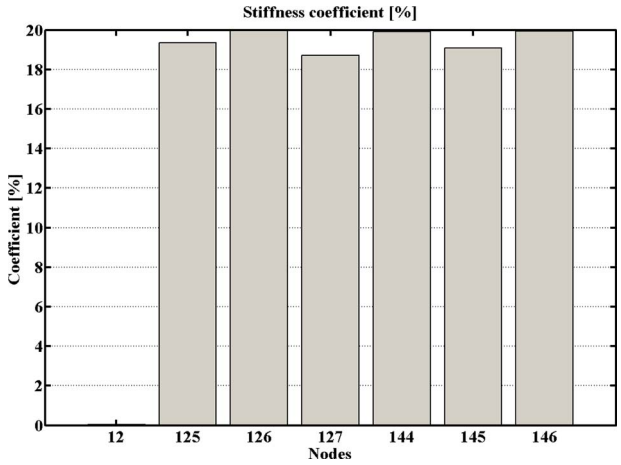

Fig. 8 Stiffness coefficient

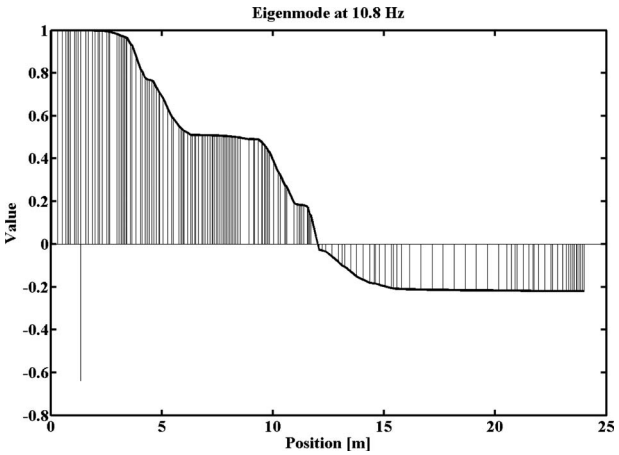

Fig. 9 First eigenmode

Similar remarks can be deduced from the second torsional eigenmode (Fig. 10): Also at this frequency, the first additional disk can be considered as uncoupled since its rotation is nearly zero while the corresponding shaft element along the rotor is characterized by a negative rotation. For the sake of brevity, third and fourth updated eigenmodes are not reported in this paper but their shapes confirm the physical reliability of the performed updating procedure.

5 Conclusion

The aim of this paper is to present torsional model updating of industrial rotating machinery. Since only the torsional natural frequencies were measured during the experimental tests, the updating procedure was based on these parameters only. A modified torsional finite element modeling for the disks was proposed in order to improve model accuracy. The selection of the updating parameters was realized by means of a sensitivity analysis based on the comparison between the experimental frequencies and the calculated eigenfrequencies.

The updating procedure was performed by imposing constraints on the variation in updating parameters in order to preserve the physical meaning of the model.

The updated model shows a good fitting of the measured torsional natural frequencies: The initial total error of 29.18% was reduced to 2.28%.

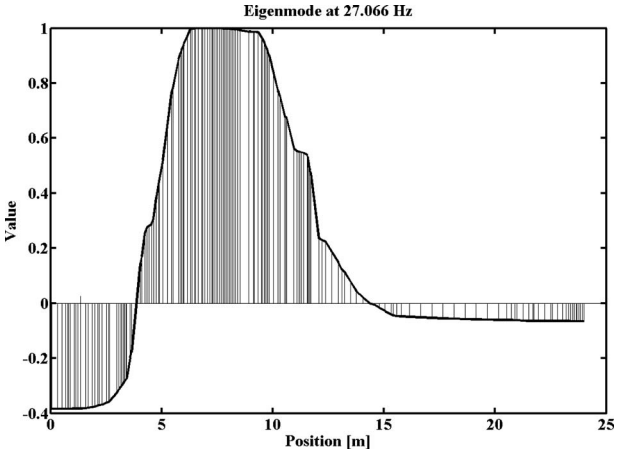

Fig. 10 Second eigenmode

The corresponding eigenmodes cannot be compared to the experimental ones because it was impossible to measure them, but the analysis of their shape suggests that they are acceptable.

References

[1] Wang, Z., and Li, D., 1994, "Modelling of Torsional Vibration of Large Turbogenerator Rotor and Its Experiment Verification," Zhongguo Dianji Gongcheng Xuebao, Proc. Chin. Soc. Electr. Eng., **14**(1), pp. 27–33.

[2] Lalanne, M., and Ferraris, G., 1998, *Rotordynamics Prediction in Engineering*, 2nd ed., Wiley, Chichester, pp. 204–206.

[3] Friswell, M. I., and Mottershead, J. E., 1995, *Finite Element Model Updating in Structural Dynamics*, Kluwer Academic, Dordrecht.

[4] Smith, S. W., 1998, "Iterative Matrix Approximation for Model Updating," Mech. Syst. Signal Process., **12**(1), pp. 187–201.

[5] Cha, P. D., and Gu, W., 2000, "Model Updating Using an Incomplete Set of Experimental Modes," J. Sound Vib., **233**(4), pp. 587–600.

[6] Levin, R. I., and Lieven, N. A. J., 1998, "Dynamic Finite Element Model Updating Using Simulated Annealing and Genetic Algorithms," Mech. Syst. Signal Process., **12**(1), pp. 91–120.

[7] Akula, V. R., and Ganguli, R., 2001, "Finite Element Model Updating for Helicopter Rotor Blade Using Genetic Algorithm," AIAA J., **41**(3), pp. 554–556.

[8] Feng, F. Z., Kim, Y. H., and Yang, B.-S., 2006, "Application of Hybrid Optimization Techniques for Model Updating of Rotor Shafts," Struct. Multidiscip. Optim., **32**, pp. 65–75.

[9] Mares, C., Mottershead, J. E., and Friswell, M. I., 2003, "Results Obtained by Minimizing Natural-Frequency Errors and Using Physical Reasoning," Mech. Syst. Signal Process., **17**(1), pp. 39–46.

[10] Adams, M. L., Jr., 2001, *Rotating Machinery Vibrations*, Marcel Dekker, New York, pp. 85–91.

[11] Rao, S. S., 2004, *Mechanical Vibrations*, 4th ed., Pearson Education, Inc., Toronto, pp. 856–862.

[12] Powell, M. J. D., 1978, "A Fast Algorithm for Nonlinearly Constrained Optimization Calculations," *Numerical Analysis* Vol. 630, (Lecture Notes in Mathematics), G. A. Watson ed., Springer, Berlin.

[13] Powell, M. J. D., 1978, "The Convergence of Variable Metric Methods for Nonlinearly Constrained Optimization Calculations," *Nonlinear Programming* Vol. 3, O. L. Mangasarian, R. R. Meyer, and S. M. Robinson, eds., Academic, New York.